

Complexity Project: The Oslo Model

CID: 01516164

20th February 2021

Word Count: 2114

Abstract

Self-organised criticality is when emergent macroscopic behaviours are invariant when scaling. To study this effect, the Bak, Tang, Wiesenfeld model was developed and later the Oslo model applied this theory to a rice pile. This project aimed to simulate this model in python using threshold conditions for the slope of the pile. The project then analysed the data from the system by first looking at the height of the pile. From this, a data collapse was found along with an understanding of the transient and recurrent configurations. The probabilities of the pile heights were calculated and plotted, and then another data collapse was performed. Next, the avalanche size probability was calculated and discussed and two methods were used to find the critical exponents.

1 Introduction

Emergence phenomena can be seen throughout nature in systems from biology to sociology. This phenomenon occurs when a system exhibits a collective behaviour that can not be understood from the rules obeyed by the individual parts of the system. Self-organised criticality is when there is a critical point at which the system undergoes a phase transition to produce macroscopic behaviours. These macroscopic results cannot be changed by changing the initial parameters. Thus, the system is invariant when scaling. The function that satisfies this scale-free behaviour is the power law.

This self-organised criticality model was first introduced metaphorically in 1987 by Bak, Tang and Wiesenfeld [1]. The Oslo model was then developed in 1996 [2] to test criticality on a physical system. The rice pile was the main focus of this project. In their paper, Frette *et al* studied the avalanches caused by adding one grain at a time to a rice pile and they measure the results after it had reached a steady-state. This investigation aimed to simulate and understand these results by using python.

The implications of the BTW model are vast. The Ising model in one dimension is analogous to the BTW and is used to understand phase transitions. It was first applied to ferromagnetism and has since been used to predict financial and social trends by taking an agent-based approach. Moreover, the Oslo model can be used to model earthquake events and to understand rainfall. The stress built up by tectonic plates can exceed a friction threshold, causing an earthquake to occur. This threshold, which after crossing produces an energy release, is what this project endeavoured to explore.

2 Implementation of the Oslo Model

The Oslo model was implemented by using an algorithm whereby when a slope of a pile was bigger than the threshold slope, a relaxation occurred. Eventually, the system reaches a steady-state and an average height. At a lattice site number of $L=16$, the average height was 26.2m, and at $L=32$ the height was 53.9m. This was concurrent with what was expected, proving the correctness of the code.

The Oslo model has two threshold slopes of either one or two. There is an equal probability that the threshold is equal to either of these slopes values at each site and the threshold value changes (with the 0.5 probability) for sites that have been relaxed. The BTW model, however, has all threshold slopes equal to one with a probability of one. So to further test the reliability of the code, the height was plotted against time for both models and Figure 1 shows their differences. The BTW model has a staircase gradient and a straight plateau at 32m for $L=32$ which was to be expected.

The Oslo model fit behaved differently to the BTW model in a way one would expect. Thus, the implementation of the model was successful.

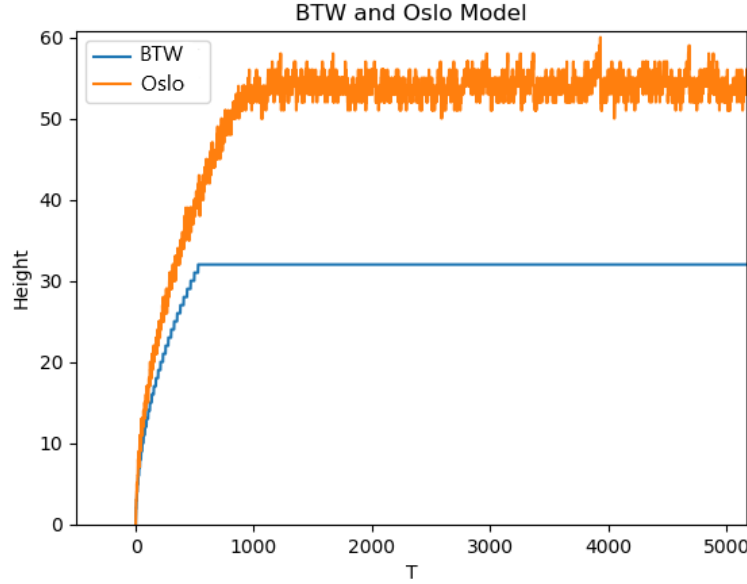


FIGURE 1: The height against time for the Oslo model and the Bak, Tang, Wiesenfeld model for a system with lattice sites $L=32$.

3 Analysing the Height of the Pile

After the successful implementation of the model, the next focus was to measure the heights of the pile. Figure 2 shows how the heights change with time for four different lattice sizes. All of the plots initially follow a curve which is the period where the system has transient configurations. When the lines plateau, the systems have reached the steady-state and have recurrent configurations.

The crossover times, t_c , in Figure 2 are the times at which the graph begins to plateau. These are the times when transient configurations become recurrent. The crossover times for $L=8, 16, 32, 64, 128$ respectively were 62s, 224s, 865s, 3370s, 13903s, and 53636s. To see how the crossover times scaled with $L \gg 1$, the moving average heights were calculated for each of these system sizes and plotted against t as shown in Figure 3.

The intercepts of Figure 3 show that the moving average heights after t_c are proportional to the length of the system. Thus, the processed pile height scales linearly with system size. Moreover, one can see that crossover time is proportional to L^2 , meaning t_c scales like L^2 .

Using these results, we introduced the scaling function,

$$h(t; L) = L^1 F\left(\frac{t}{L^2}\right) \quad (1)$$

Then plotted the average height divided by L against the time divided by L^2 to get the data collapse in Figure 4.

By looking at the change in gradient in Figure 4, one can see that for $L \gg 1$ there is a much sharper transition. We can also see that $F(\frac{t}{L^2})$ follows a power law when $(\frac{t}{L^2}) \ll 1$,

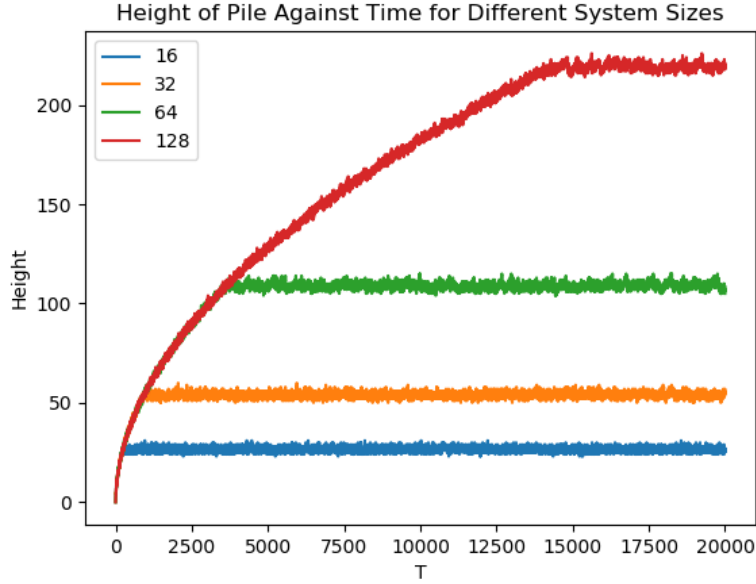


FIGURE 2: The height of the pile plotted against time for four different systems with a number of sites, $L = 16, 32, 64, 128$.

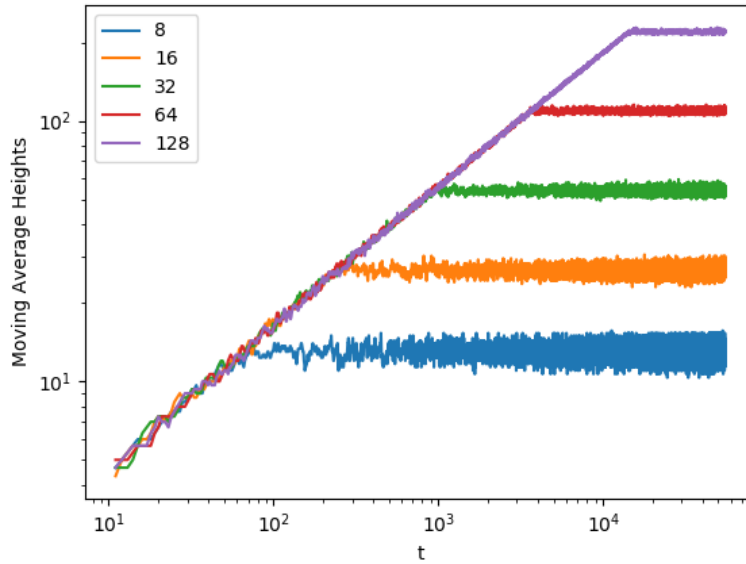


FIGURE 3: The moving average of the heights of the pile against t for different system sizes.

and $F(\frac{t}{L^2})$ is constant when $(\frac{t}{L^2}) \gg 1$. This demonstrates a phase transition, which is a crucial feature of self-organised critically in application. Therefore, because the transient state occurs when $(\frac{t}{L^2}) < 1$, we can show that the average height increases with t in the transient state by fitting a power law to the data as seen in Figure 5. This is scale invariant.

The average height of the pile once the system has reached the steady-state was plotted

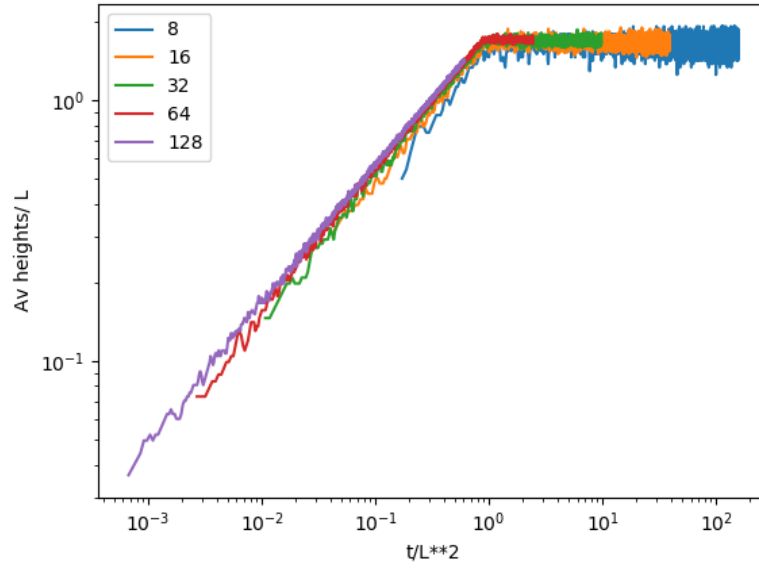


FIGURE 4: The data collapse for the processed height $\tilde{h}(t; L)$ vs. time t for the various system sizes.

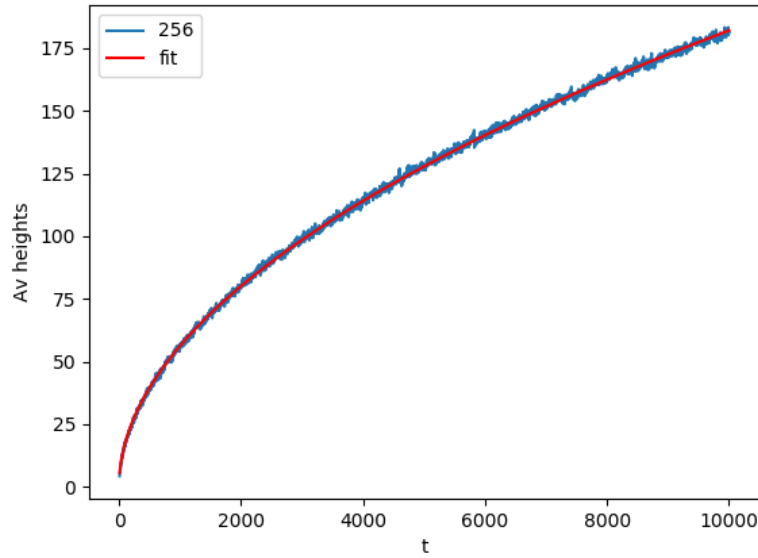


FIGURE 5: The transient state data of a lattice of size $L = 256$. The average height is plotted against time and a power law curve function is fitted to the data.

against system size on a log scale. By zooming in on this graph as shown in Figure 6, it shows signs of corrections to scaling when L is small. The function used to fit to the data was,

$$\langle h \rangle = a_0 L (1 - a_1 L^{-w_1}) \quad (2)$$

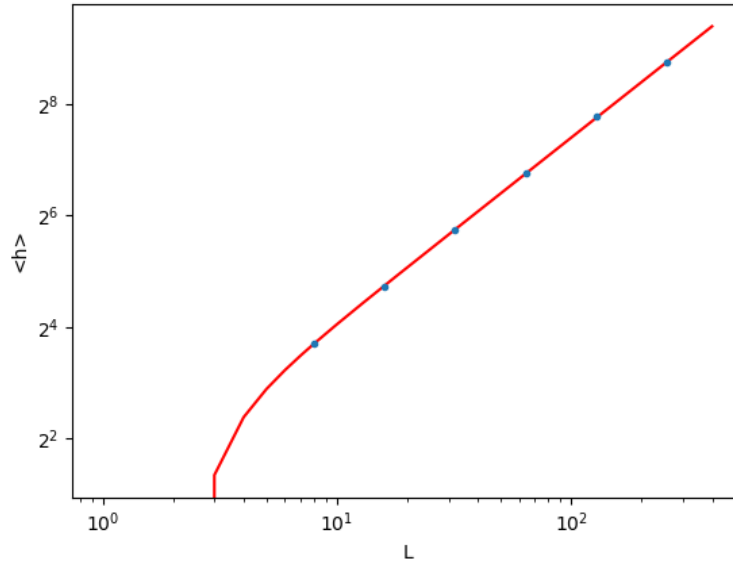


FIGURE 6: Average height of the pile against L with the curve fit function from Equation 2. Shows signs of corrections to scaling.

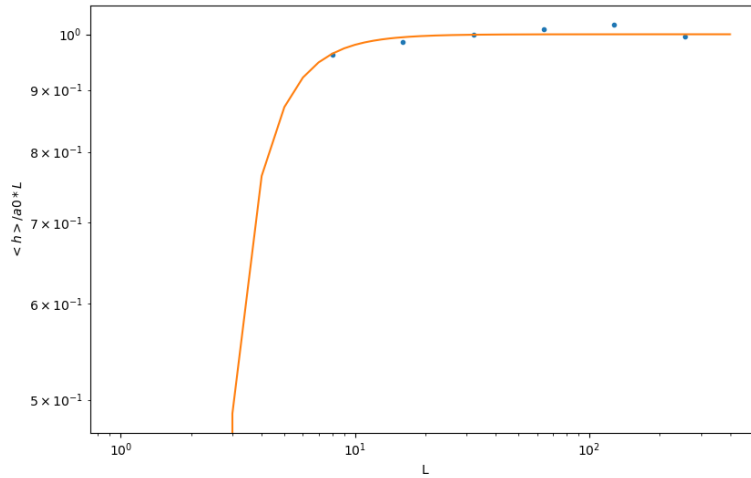


FIGURE 7: $\frac{\langle h \rangle}{a_0 L}$ plotted against L on a log scale.

Fitting this correction to scaling returned the parameters with values; $a_0 = 1.68$, $a_1 = 1.93$ and $w_1 = 1.88$. a_0 is also equal to the plateau of the average slope after data collapse in Figure 4. To see how well these parameters fit, $\frac{\langle h \rangle}{a_0 L}$ was plotted against L on a log scale as seen in Figure 7. By plotting it this way, one can expose the corrections to scaling even for larger values of L .

In Figure 8, the standard deviation of the height against system size was plotted and a

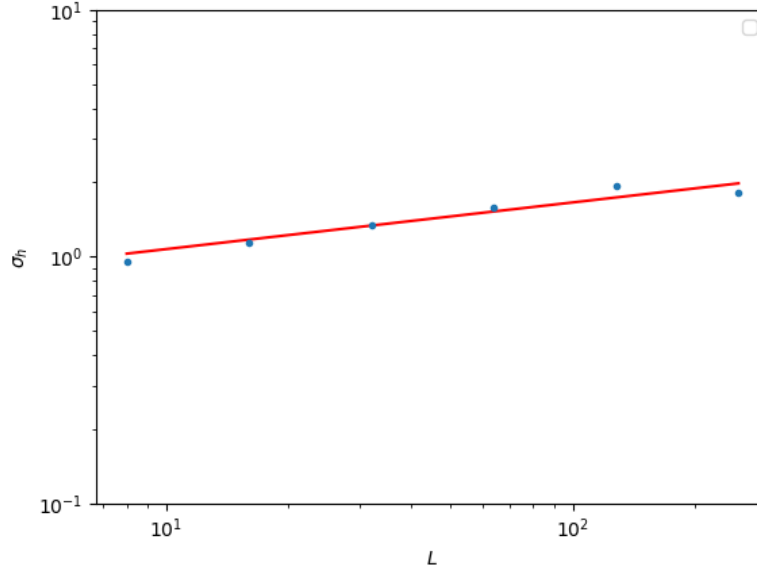


FIGURE 8: The standard deviation of the height of the pile against system size.

power law function in Equation 3 was used to fit the curve,

$$\sigma_h(L) = nL^w \quad (3)$$

This returned the parameters $n = 0.599$ and $w=0.24$. Since the height of the pile can be defined as the sum of the slopes at each lattice site. The standard deviation of the slopes, σ_z is then σ_h divided by the system size. This means σ_z is proportional to L^{w-1} and so when L tends to infinite, σ_z tends to zero. We could then scale the standard deviation of the height as shown in Figure 9.

Next, the probability of the height was calculated for each system size and can be seen in Figure 10. This was done by summing the total observed configurations at a height divided by the total number of configurations. It was to be expected that each lattice size would have height probabilities that were mutually independent with the same probability distribution. This is because the slopes are independent and identically distributed. Due to the relationship between height and slope, we also expected our probability density function to be a normal distribution which is seen in Figure 10.

The amplitudes of the peaks in Figure 10 follow an inverse power law. Moreover, the difference along the x axis of the distributions is the average height pile for each lattice size. Therefore, to produce a data collapse of the height probabilities as seen in Figure 11, we used the scaling function,

$$P(h; L) = L^{-w} F((h - \langle h \rangle) L^{-w}) \quad (4)$$

This produced a Gaussian distribution that was slightly asymmetric, which was seen when plotting the y-axis on a logarithmic scale. The deviations from the Gaussian shape

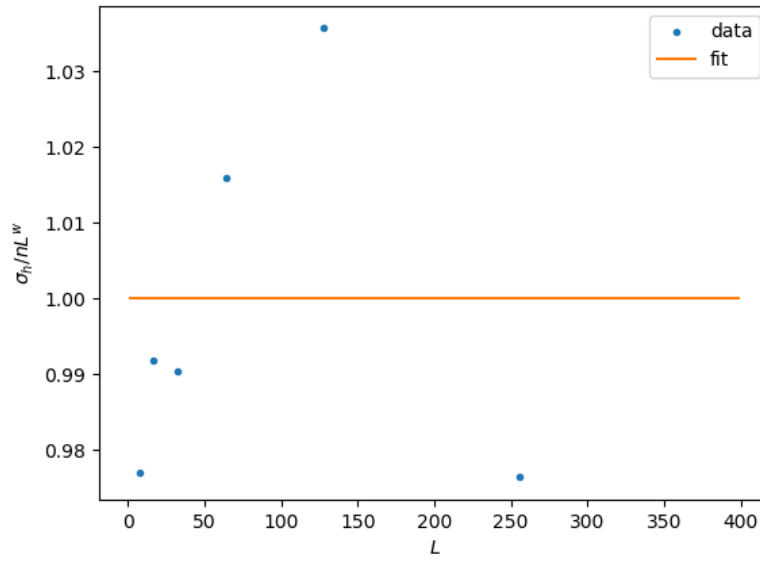


FIGURE 9: The standard deviation of the height of the pile divided by nL^w against system size.

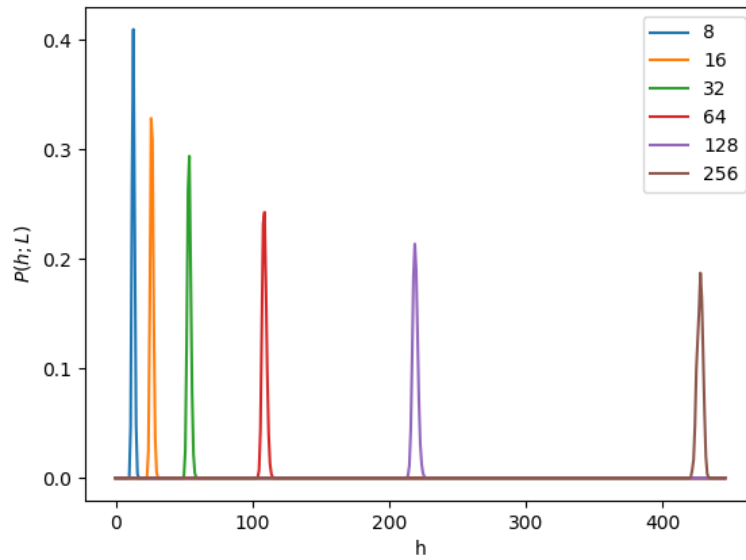


FIGURE 10: The height probability of different system sizes plotted against height.

appeared to be for smaller values of L . The ability to achieve this data collapse implies the system has universality.

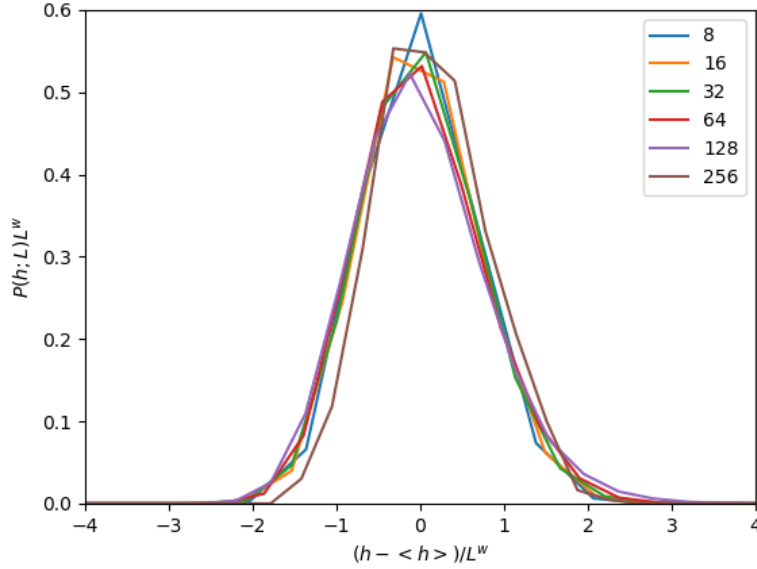


FIGURE 11: The data collapse of the height probability of different system sizes. Achieved by plotting $L^w P(h; L)$ against $(h - \langle h \rangle)L^{-w}$.

3.1 Analysing the Avalanche Size Probability

The avalanche size is the number of relaxations in the system after a grain is added. The probability of an avalanche was calculated the same way as the height probability; the number of avalanche configurations, s , divided by the total number of configurations (after the system had reached the steady state). The log-binned data was used to plot Figure 12 with a scale factor of 1.3 chosen through trial and error to produce a smooth curve. The behaviour of the different system sizes in Figure 12 seemed to be similar. This similarity of shape alludes to universal behaviour which we next try to identify using finite-size scaling.

Looking at Figure 12 also shows that in the middle of each line plotted there is a region that follows a power law. To show this, a power law function was fitted on Figure 13 with system size $L=128$. The function $j s^{t_s}$ gave the parameters $j = 0.33$ and $t_s = -1.52$. This was used on the middle of the graph, because at just before $s = 10^4$, the avalanche size starts to decay rapidly so there is a cut-off avalanche size. This cut-off appears to systematically increase with system size. Figure 14 resembles the data for the annual number of earthquakes of size S against S on a logarithmic scale, showing how useful this research can be.

To test the scaling function,

$$\tilde{P}N(s; L) s^{t_s} G \frac{s}{L^D} \quad (5)$$

we first plotted $s^{t_s} P_N(s; L)$ against s . Then Figure 14 was plotted with trial and error to deduce the value for D that would ensure the best data collapse. To produce this figure

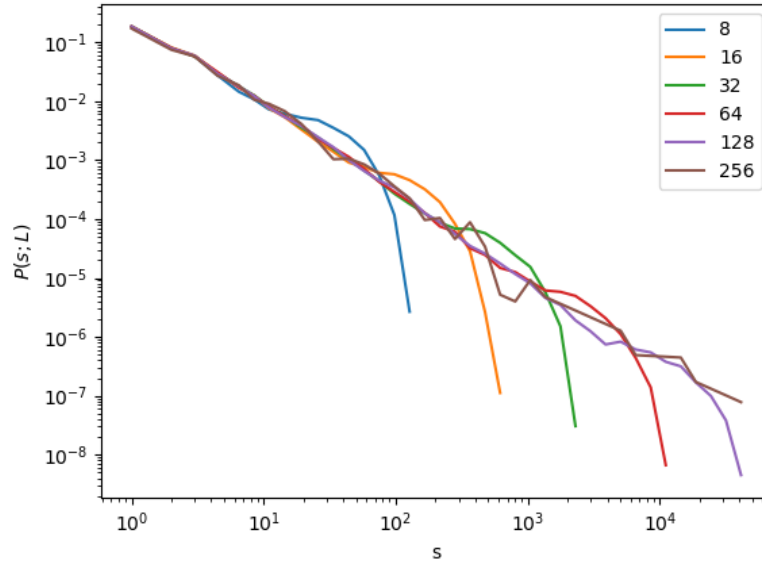


FIGURE 12: The probability of an avalanche of size s against avalanche size for different systems sizes. The data was log-binned with a sample size of $N = 100000$

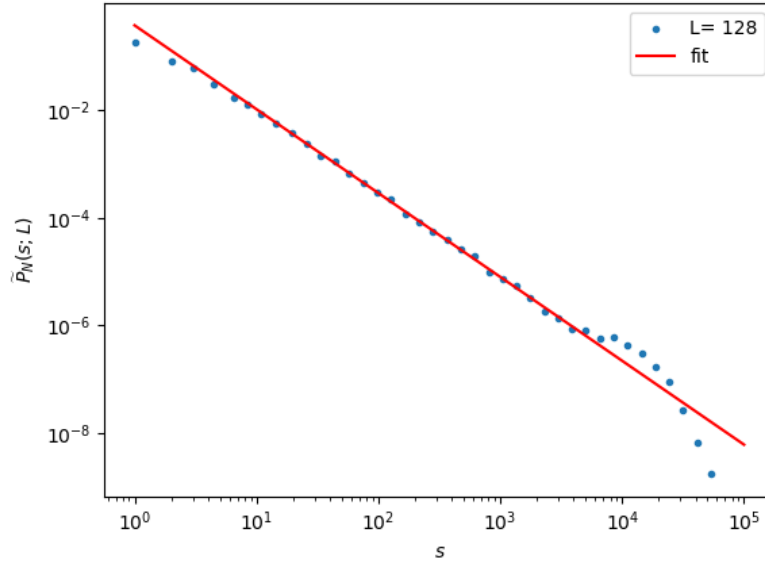


FIGURE 13: Avalanche probability against height for a system size of $L = 128$. A power law function is fitted to the middle of the curve.

$D=2.12$ was used. This value also satisfies the scaling of the BTW model $D(2 - t_s) = 1$. This scaling function demonstrated universality, where it can explain avalanche probability

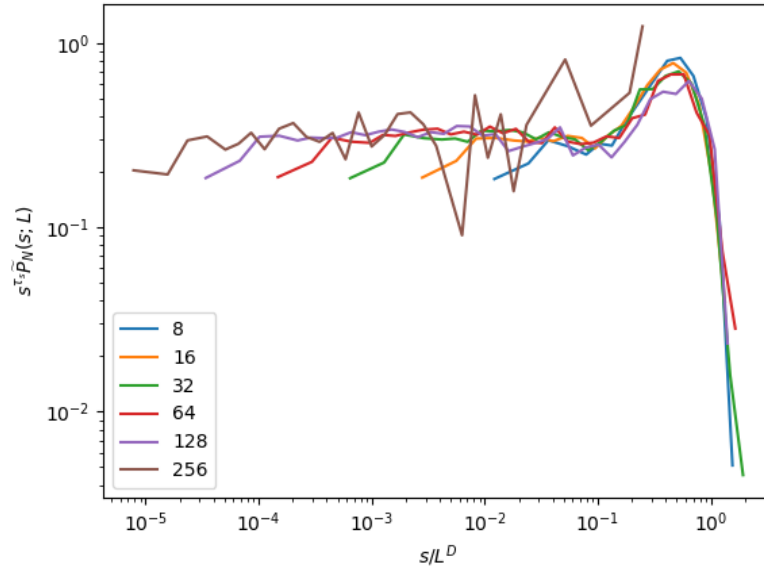


FIGURE 14: The caption goes under the figure like this. Note that textwidth is the width of the text. But you can use any units, e.g., “3in” or “50mm”.

for all system sizes. Next, the k th moment was measured using,

$$\langle s^k \rangle = \lim_{T \rightarrow \infty} \frac{1}{T} \sum_{t=t_0+1}^{t_0+T} s_t^k \quad (6)$$

$\langle s^k \rangle$ was plotted against L in Figure 15 to show that $\langle s^k \rangle$ scales with linear regression.

We can use these values to devise another method of determining t_s and D . In Figure 16, the linear regression curve fit function was applied on the log scale. This returned a value for t_s of 1.61 and a value for D of 2.42. These are the two critical exponents which describe the behaviour near the phase transition. They are believed to be universal, though it has not been proven. This was done using the equation,

$$\log \langle s^k \rangle = D(1 + kt_s) \log L + \log(\text{constant}) \text{ for } L \gg 1, k \gg 1 \quad (7)$$

then by plotting the slopes of k against k as shown in Figure 17.

The last point in Figure 17 was not included in the curve fit, because it does not follow the trend. This is at $L=256$ and might be wrong due to the numbers being too high. The computer has a maximum precision for numbers it can store. Therefore, the curve function was only applied to $L=64$ and 128 . It must be done for $L \gg 1$ as small L will show signs of correction to scaling as discussed earlier. If the results in this project had larger system sizes they would be more reliable because when L tends to infinity we can safely ignore these corrections to scaling. This could be an explanation for the difference in values for the two procedures.

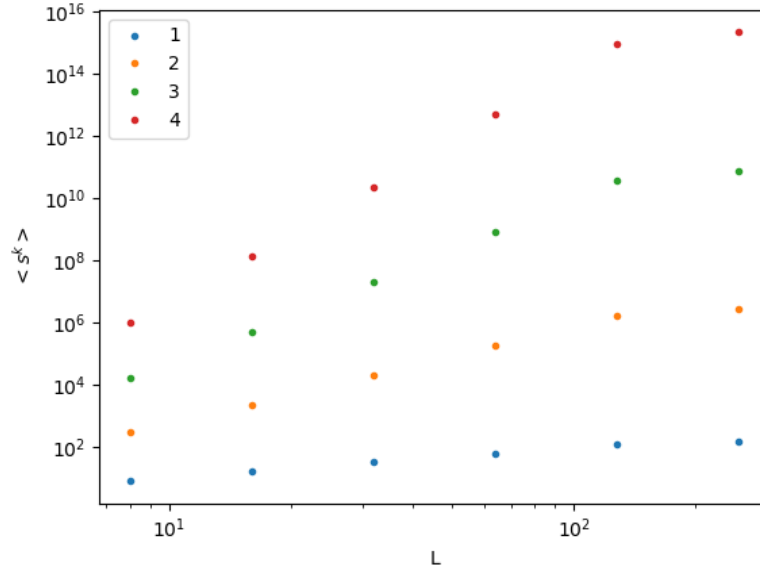


FIGURE 15: $\langle s^k \rangle$ against L for k values of $k = 1, 2, 3, 4$.

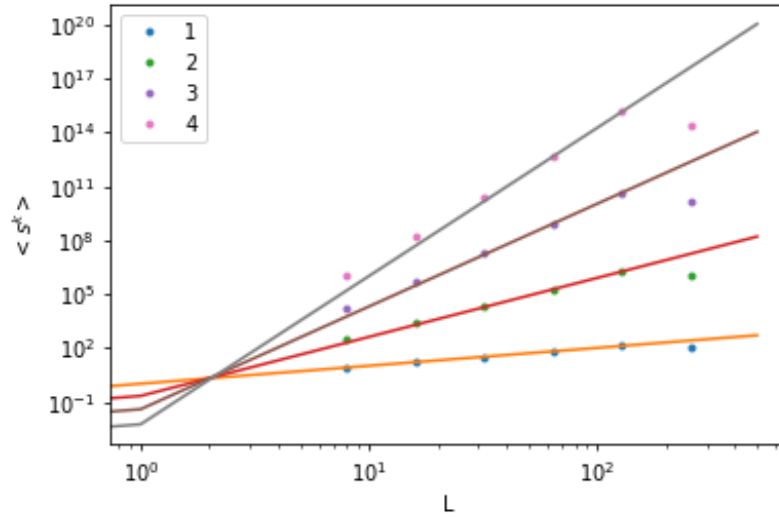


FIGURE 16: $\langle s^k \rangle$ against L for k values of $k = 1, 2, 3, 4$. A linear regression curve fit for the log scale is applied.

That being said, the moment analysis method can be advantageous as it is based on averages and is more controlled than the data collapse method. In Figure 17, D is the gradient and t_s is the intercept.

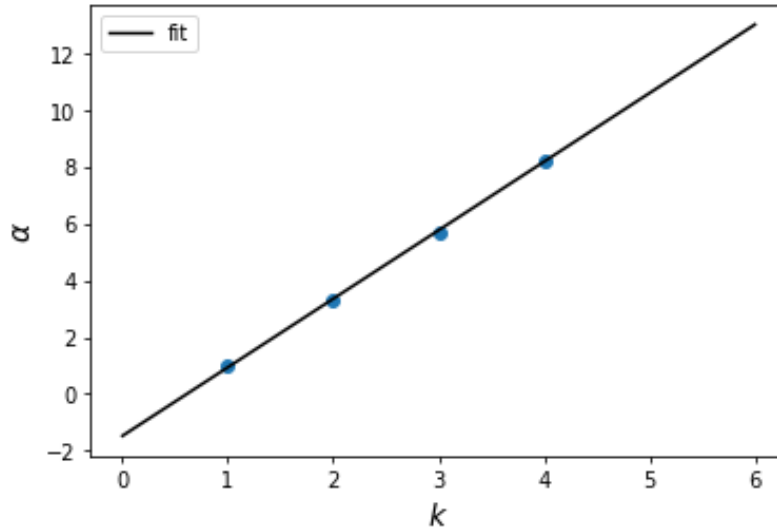


FIGURE 17: The slopes of k , α , plotted against k .

3.2 Conclusion

The aim of this experiment was to simulate and understand the properties of the Oslo model. The algorithm was successfully implemented and tested, so could be confidently used for analysis.

The first stage of analysis was to look at the height of the pile. The project found the trends for the transient and recurrent configurations and showed that there was a sharp transition between the two, meaning a phase transition occurred. We performed a data collapse for the moving average heights. The project found that there was a correction to scaling for small values of L and the standard deviation of the height followed a power law, which is a feature of scale invariance. The probability of the height of the pile was then calculated and was found to have a slightly asymmetric Gaussian shape after data collapse. The ability to use a scaling function on the probability of the height implied universality.

The project then calculated and analysed the avalanche size probability. The probability was found using the log-binned data to produce a smooth trend. The trends of the probabilities for the different system sizes were analysed. We found that the centre of the graph fit a power law and used this to perform a data collapse and find values for the critical exponents. Then the method of moment analysis was used to determine the critical exponents and the results were compared.

The project found key features of the Oslo model including; phase transition information, scale invariance, universality and the critical exponents. These features have numerous important theoretical applications spanning over a huge array of fields. To improve this project, the data for the larger values of L would be better, perhaps by using more efficient code or larger computers that could produce these larger data sets.

References

- [1] P. Bak, C. Tang, and K. Wiesenfeld, “Self-organized criticality: An explanation of the $1/f$ noise,” *Phys. Rev. Lett.*, vol. 59, no. 4, pp. 381–384, Jul. 1987, doi: 10.1103/PhysRevLett.59.381.
- [2] P. M. Gleiser, “Damage spreading in a rice pile model,” in *Physica A: Statistical Mechanics and its Applications*, Jun. 2001, vol. 295, no. 1–2, pp. 311–315, doi: 10.1016/S0378-4371(01)00094-2.